Earth's Future

Impacts of AMOC Collapse on Monsoon Rainfall: A Multi-Model Comparison

M. Ben-Yami[1,2] ⬛, P. Good[3], L. C. Jackson[3] ⬛, M. Crucifix[4] ⬛, A. Hu[5] ⬛, O. Saenko[6] ⬛, D. Swingedouw[7] ⬛, and N. Boers[1,2,8] ⬛

[1]Earth System Modelling, School of Engineering and Design, Technical University of Munich, Munich, Germany, [2]Potsdam Institute for Climate Impact Research, Potsdam, Germany, [3]Met Office, Exeter, UK, [4]Earth and Life Institute, UCLouvain, Louvain-La-Neuve, Belgium, [5]Climate and Global Dynamics Lab, National Center for Atmospheric Research, Boulder, CO, USA, [6]SEOS, University of Victoria, Victoria, BC, Canada, [7]Environnements et Paléoenvironnements Océaniques et Continentaux (EPOC)—Université de Bordeaux, Pessac, France, [8]Department of Mathematics and Global Systems Institute, University of Exeter, Exeter, UK

Abstract A collapse of the Atlantic Meridional Overturning Circulation (AMOC) would have substantial impacts on global precipitation patterns, especially in the vulnerable tropical monsoon regions. We assess these impacts in experiments that apply the same freshwater hosing to four state-of-the-art climate models with bistable AMOC. As opposed to previous results, we find that the spatial and seasonal patterns of precipitation change are remarkably consistent across models. We focus on the South American Monsoon (SAM), the West African Monsoon (WAM), the Indian Summer Monsoon (ISM) and the East Asian Summer Monsoon (EASM). Models consistently suggest substantial disruptions for WAM, ISM, and EASM with shorter wet and longer dry seasons (−29.07%, −18.76%, and −3.78% ensemble mean annual rainfall change, respectively). Models also agree on changes for the SAM, suggesting rainfall increases overall, in contrast to previous studies. These are more pronounced in the southern Amazon (+43.79%), accompanied by decreasing dry-season length. Consistently across models, our results suggest a robust and major rearranging of all tropical monsoon systems in response to an AMOC collapse.

Plain Language Summary The Atlantic Meridional Overturning Circulation (AMOC) is a key element of the Earth's climate system, transporting large amounts of heat and salt northward in the upper layers of the Atlantic Ocean. Although its likelihood remains highly uncertain, a collapse of the AMOC in response to anthropogenic climate change would have catastrophic ecological and societal consequences. This is especially true in the vulnerable monsoon regions of the tropics. Yet, the precise effects of an AMOC collapse on the tropical monsoon systems remain unclear. We take advantage of a climate model intercomparison project, and provide a detailed and systematic analysis of the seasonal impacts of an AMOC collapse on the major tropical monsoon systems. We find remarkable, previously unseen, agreement between four independent state-of-the-art climate models. Consistently across models, our results suggest major rearranging of all tropical monsoon systems in response to an AMOC collapse.

1. Introduction

The Atlantic Meridional Overturning Circulation (AMOC) is a key element of the Earth's climate system, transporting large amounts of heat and salt northward in the upper layers of the Atlantic Ocean. Paleoclimate proxy evidence as well as theoretical considerations suggest that the AMOC is bistable, with a second, substantially weaker circulation mode in addition to the present strong mode (Henry et al., 2016; Rahmstorf, 2002; Stommel, 1961). This potential bistability would be the result of the salt-advection feedback that sustains the current, strong, circulation: if the AMOC weakens, less salt is transported northwards, and the northern deep water formation is reduced, leading to an even weaker AMOC. Such self-perpetuating weakening can lead to a persistent or (meta) stable weak AMOC state with greatly reduced northern deep water formation, with reduced circulation in the Atlantic.

The question whether the AMOC is bistable in comprehensive climate models has been intensely debated in recent years, and many Global Circulation Models (GCMs) exhibit a bistable AMOC (Y. Liu et al., 2014; W. Liu et al., 2017; Jackson & Wood, 2018; Romanou et al., 2023). Concerns have been raised that the AMOC might transition to a weak state in response to enhanced freshwater inflow into the North Atlantic due to anthropogenic

warming and the resulting strengthened hydrological cycle as well as sea ice and Greenland ice sheet melting (W. Liu et al., 2017). However, the 6th assessment report of the International Panel on Climate Change (IPCC) concludes that there is medium confidence that such a transition will not happen before 2100 (Arias et al., 2021). In this work we will call a change in AMOC strength an AMOC collapse when it is a transition from the current strong circulation state to a different, weaker (meta)stable state. This terminology is thus independent of the scale of AMOC weakening, as long as that weakening is substantial.

Studying a potential AMOC collapse is of great interest given the severe global impacts it would have (Jackson et al., 2020; W. Liu et al., 2020; Weijer et al., 2019). There are several lines of paleoclimate proxy-based evidence suggesting that the AMOC has indeed weakened in the last millennium (Caesar et al., 2021) and observational proxy-based evidence that it has weakened in the last century (Bryden et al., 2005; Caesar et al., 2018; Zhu et al., 2023). Although this historical decline is controversial (Kilbourne et al., 2022; Latif et al., 2022), comprehensive models predict that the AMOC will weaken under anthropogenic global warming (Lee et al., 2021). In addition, evidence that the recent AMOC weakening might be associated with a decrease of stability of the current circulation mode has been identified in sea-surface temperature (SST) and salinity based fingerprints of the AMOC strength (Ben-Yami et al., 2023; Boers, 2021).

If the AMOC were to collapse, the reduced northward ocean heat transport would cause a relative cooling of the northern hemisphere, and the change in inter-hemispheric energy transport would lead to a shift of the thermal equator and hence a southward shift of the inter-tropical convergence zone (ITCZ) (Donohoe et al., 2013; Frierson et al., 2013; T. Schneider et al., 2014). The subsequent global-scale reorganization of the atmospheric circulation would have far-reaching effects in the Pacific as well as in the Atlantic (Orihuela-Pinto et al., 2022). As the ITCZ is strongly linked to tropical rainfall, an AMOC collapse and associated southward ITCZ shift would likely have substantial consequences for monsoon systems (Good et al., 2021). Given their socioeconomic and ecological importance, a detailed analysis of the impacts of an AMOC collapse on these monsoon systems is needed. Over half of the world's population live in climates dominated by tropical monsoons (Moon & Ha, 2020; Wang et al., 2021). Most of these are in developing countries, where land use is dominated by agriculture, so depends heavily on the rain the monsoons bring. These regions are thus vulnerable to any changes in the characteristics of the monsoon rains, whether they are changes in the timing or the amount of rainfall (WRCP, 2023). This makes tropical monsoon regions a high priority regarding possible impacts of anthropogenic global warming (Wang et al., 2021).

There exist multiple lines of proxy evidence to assess the impacts of an AMOC collapse on the tropical monsoon systems during past climate conditions (Häggi et al., 2017; Marzin et al., 2013; Mosblech et al., 2012; Sandeep et al., 2020; Sun et al., 2012; Wassenburg et al., 2021). To study the effects in more detail and for present-day climate conditions, so-called hosing experiments in general circulation models (GCMs) are used, in which freshwater is added to a region of the north Atlantic for a long period of time, forcing the AMOC to weaken and potentially collapse to a weaker state. Some studies have also focused on individual monsoon systems such as the South American Monsoon (SAM) (Good et al., 2021; Parsons et al., 2014), the West African Monsoon (WAM) (Chang et al., 2008; Defrance et al., 2017), the Indian Summer Monsoon (ISM) (Marzin et al., 2013; Sandeep et al., 2020) and the East Asian Summer Monsoon (EASM) (Yu et al., 2009). Most of these studies find an overall decrease in annual mean precipitation of the different monsoon systems. For tropical South America, however, older simulations suggesting increased annual rainfall sums (Stouffer et al., 2006) are in contrast with more recent modeling studies suggesting decreases (Jackson et al., 2015). In addition, both Parsons et al. (2014) and Good et al. (2021) note that it is important to analyze the atmospheric response throughout the seasonal cycle. Specifically, Parsons et al. (2014) find that a wetter dry season after an AMOC collapse increased the overall Amazon vegetation productivity. The overall sign of the precipitation change over tropical South America in response to an AMOC collapse remains debated. This debate is complicated by the fact that there has been no inter-model AMOC hosing comparison since Stouffer et al. (2006), and in general it is difficult to compare the impacts in experiments with different hosing scenarios. In addition, Stouffer et al. (2006) used much older, lower-resolution models that are less reliable for simulations of regional precipitation (Guiling et al., 2017; Strandberg & Lind, 2021; Yu et al., 2009), and only showed the annual mean changes in rainfall over the Atlantic and surrounding land. There is thus a need for an updated and more detailed assessment of the impacts of an AMOC collapse on monsoon precipitation.

The bi-stability of the AMOC has long been supported by theory and by simple and intermediate-complexity models (Rahmstrof et al., 2005; Stommel, 1961), and is often judged consistent with abrupt shifts in
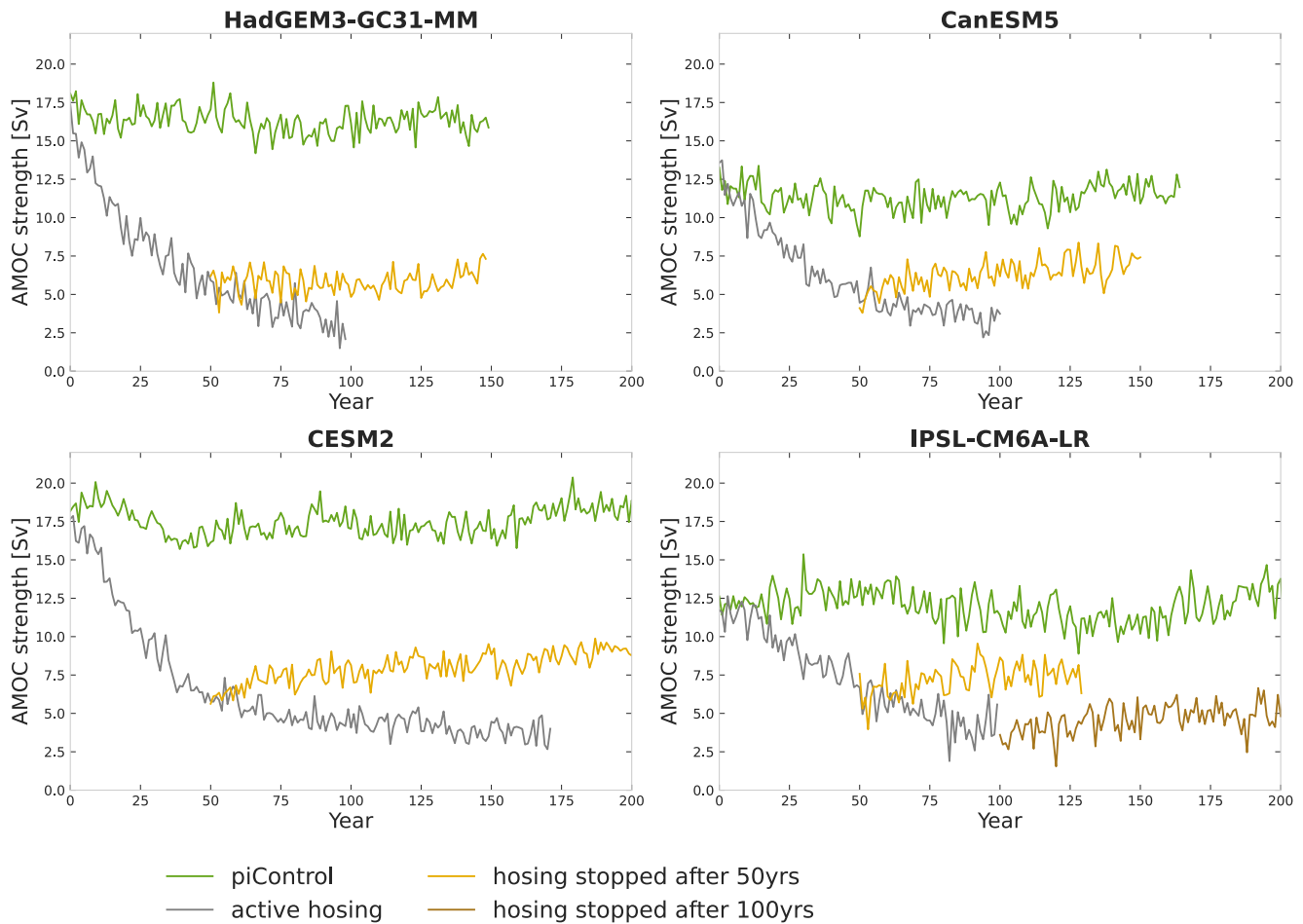
Figure 1. Yearly average Atlantic Meridional Overturning Circulation (AMOC) strength at 26.5°N for the four model experiments: (a) HadGEM3, (b) CanESM, (c) CESM, and (d) IPSL. The piControl strength is shown in solid green and the active hosing strength in gray. The post-hosing AMOC strength is shown in solid gold (brown) if the hosing is stopped after 50 (100) years. The full timeseries are shown, out of which only 80 years are used in this work.

circulation identified in the paleoclimate data record (Henry et al., 2016; Rahmstorf, 2002). Nevertheless, many GCMs do not exhibit the hysteresis associated with bi-stability (Drijfhout et al., 2011; Y. Liu et al., 2014), although more recent studies do find a persistent weak state in some GCMs (Jackson & Wood, 2018; Romanou et al., 2023). The North Atlantic Hosing Model Intercomparison Project (NAHosMIP) compares eight different models from the sixth phase of the Climate Model Intercomparison Project (CMIP6), aiming to investigate AMOC response and associated hysteresis (Jackson et al., 2022). Not only is the same hosing strength used for all four models, but the bistability of the AMOC in some of the models allows us to investigate the impacts of their transition to the stable weak AMOC state (Figure 1). This stable weak state persists for at least 100 years, meaning that these impacts are irreversible at least over a human lifetime, if not longer. This is in contrast to most AMOC hosing studies, in which the hosing is continuouously applied during the study period. In the following, we will refer to the post-hosing, collapsed state, as the weak AMOC.

The different models of NAHosMIP exhibit a range of different patterns and biases, and thus comparing the effect of an AMOC collapse across models allows us to make robust statements on its effect on tropical precipitation. In this study we use results from the four models in NAHosMIP that remain in the weak state after the hosing is stopped, suggesting this weak state is dynamically stable: HadGEM3-GC31-MM, CanESM5, CESM2, and IPSL-CM6A-LR (hereafter abbreviated as HadGEM, CanESM, CESM, and IPSL, see Figure 1). We compare spatial precipitation fields from pre-industrial control runs of these models (piControl) to scenarios in which a constant 0.3 Sv of hosing is applied over the North Atlantic for 50 years (100 years for the IPSL model), thus weakening the AMOC. This allows us to study the impacts of an AMOC collapse using AMOC states that remain weak for at

least a hundred years without any forcing. This is preferable to the standard method of studying a weak AMOC state where the hosing is still ongoing, as hosing is by definition unphysical, and the addition of such large quantities of freshwater to the ocean can have unforeseeable effects on the climate that are not a direct consequence of the weakening of the AMOC. We thus did not use the other four models from NAHosMIP, as they had no stable weak AMOC state in the experiments.

This study is the first since Stouffer et al. (2006) to compare the impacts of an AMOC collapse across multiple models, and is the first to do so with experiments where the same hosing strength and location is applied across models. In addition, we extend the standard analysis of the mean annual precipitation (Jackson et al., 2015; Stouffer et al., 2006) to a detailed analysis of the seasonal changes. We are thus able to provide novel information in all four monsoon regions, detailing the changes in the seasonal cycle both regionally and locally. The nuances in the seasonal changes are especially important in the context of the societal and ecological impacts of an AMOC collapse.

2. Results

### 2.1. Global Change in Precipitation

Since the models have biases with respect to observations from the GPCP precipitation data set (Adler et al., 2016) (Figure S1 in Supporting Information S1), one cannot compare the post-hosing runs to observations. To understand the effect of an AMOC collapse on global precipitation, we therefore analyze the differences between the post-hosing and pre-industrial control runs of the same models.

The resulting pattern of global precipitation shifts in response to an AMOC collapse is then remarkably similar in all four models (Figures 2a–2d and Figure S2 in Supporting Information S1): (a) a southward shift of the ITCZ and overall increased (decreased) precipitation over the southern (northern) hemisphere; (b) a general reduction of precipitation of the higher latitudes of the northern hemisphere; (c) reduced precipitation in all defined monsoon regions except the SAM; and (d) increased precipitation over most of the Amazon, especially in the east.

The four models show a remarkable agreement on the sign of precipitation changes in the tropics (20°S–20°N) in response to an AMOC collapse. The fraction of land in which the sign of change is consistent in the four models is 0.64 in the tropics, and is as large as 0.95 and 0.99 in the ISM and WAM (see Table S1 in Supporting Information S1 and Figure 3). The agreement in the seasonal cycle change is also especially high in the Atlantic monsoon regions (Table S3 in Supporting Information S1). As this study is the first quantitative intercomparison of hosing experiments, we use CMIP6 runs to provide context for these numbers. Notably, in the tropics the agreement between these four models on the impacts of an AMOC collapse are consistently higher than the agreement found in different CMIP6 warming experiments (Figure 3). This is likely due to the fact that an AMOC collapse leads to large-scale changes in precipitation patterns, whilst higher temperatures lead to more complex regional changes. However, as noted above, there have been large differences between the results of hosing experiments with previous generations of models (Jackson et al., 2015; Stouffer et al., 2006). As CMIP6 models are known to still have inconsistent precipitation projections in the tropics for increases in CO_2 (Fiedler et al., 2020; Moon & Ha, 2020; Wang et al., 2021), the higher agreement found in the hosing experiments is remarkable.

Whilst the overall pattern of change in the four models subsequent to an AMOC collapse is in agreement, the magnitude of the precipitation change varies. CanESM and IPSL have a comparably small change in precipitation following an AMOC collapse, of the order of 0.5 mm/day in the monsoon regions (Figure 2). The model with the largest precipitation change is CESM, with a precipitation change over the SAM, ISM, and WAM in CESM of the order of 2–3 mm/day, with a slightly smaller change in the EASM. HadGEM is midway between the two extremes with changes on the order of 1 mm/day. HadGEM also has a more complex precipitation change pattern for the SAM, with less rainfall over about half of the northern Amazon region and more rainfall over the rest of the region.

Even in light of the differences in magnitude, the agreement between the models is remarkable, given that previous generations of models have shown considerably stronger differences and inconsistencies. For example, Jackson et al. (2015) showed a drying over almost all of the Amazon, in contrast to the multi-model comparison in Stouffer et al. (2006). The fact that the models agree in general on the pattern of precipitation change allows us to examine this pattern in the ensemble mean (Figure 4). As we only have four models, this ensemble mean should not be taken as being an accurate prediction, but rather as a tool to showcase the pattern of precipitation change where the models agree (black stippling in Figure 4). Thus the ensemble mean shows the overall same pattern as
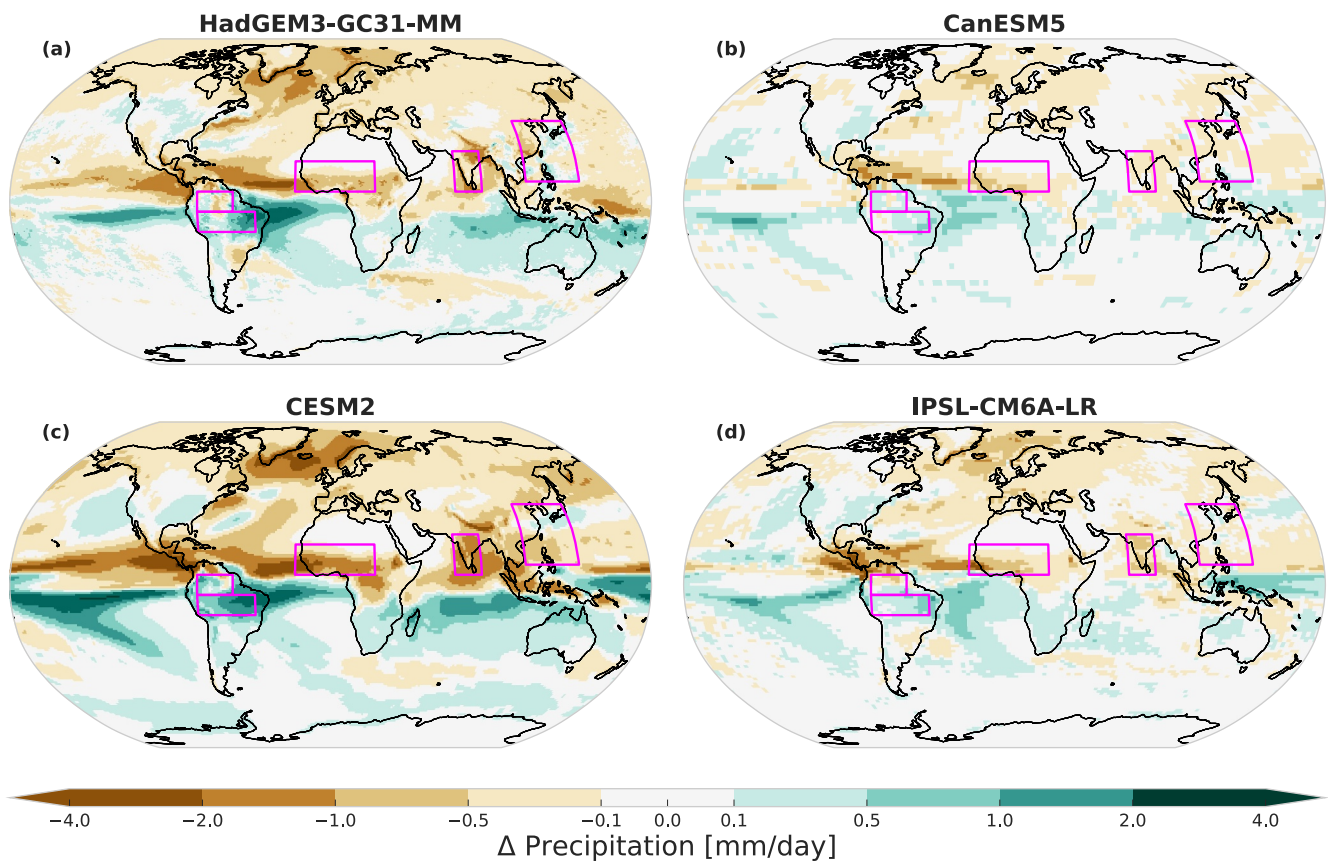
Figure 2. Modeled impacts of an Atlantic Meridional Overturning Circulation (AMOC) collapse on global precipitation. Mean annual precipitation shifts (weak AMOC run minus piControl run) for (a) HadGEM3, (b) CanESM, (c) CESM, and (d) IPSL. Note the southward inter-tropical convergence zone shift and the general pattern of Northern-Hemisphere drying and Southern-Hemisphere wettening in response to an AMOC collapse, shared by all models. The magenta boxes show the monsoon regions investigated in this work: the two parts of the South American Monsoon as well as the West African Monsoon, Indian Summer Monsoon, and East Asian Summer Monsoon (see Section 4 and Table S2 in Supporting Information S1).

described above, with a drying of all monsoon regions except the SAM. The ensemble mean percentage changes in rainfall in the monsoon regions are (Figure S2 in Supporting Information S1): +5.2% in the Northern Amazon, +43.79% in the Southern Amazon, −29.07% in the WAM, −18.76% in the ISM and −3.78% in the EASM.

Although it is not a focus of this work, the models also agree to some extent on the precipitation changes over the southeastern Asian monsoon system (see Figure S3 in Supporting Information S1). With the exception of IPSL, there is a decrease in precipitation over land in the north and an increase in the south. On the other hand, there is less agreement on the precipitation change over the surrounding ocean, with no coherent pattern to the change. This is also reflected in the calculations of model agreement, which show much less agreement in that area than in the other monsoon boxes (Figure S4 in Supporting Information S1).

To understand the different magnitudes of model responses to an AMOC collapse we analyze the seasonal cycle of the Atlantic ITCZ following Good et al. (2021) (see Section 4). A smaller shift of the Atlantic ITCZ after an AMOC collapse should result in a smaller precipitation anomaly, and this is reflected in the respective Atlantic ITCZ shifts of the models (Figures S5a–S5d in Supporting Information S1). IPSL and CanESM have only a small (≤1°) latitudinal shift in the Atlantic ITCZ between the control and weak AMOC, whilst the shift in HadGEM and CESM is a few times larger. The latter two also have a seasonal Atlantic ITCZ cycle which is closer to the observations (see Section 4 for details). The ordering of magnitudes is also mirrored in the amount the model AMOC weakens from the piControl to the weak state in the respective models (Figure S6 in Supporting Information S1).
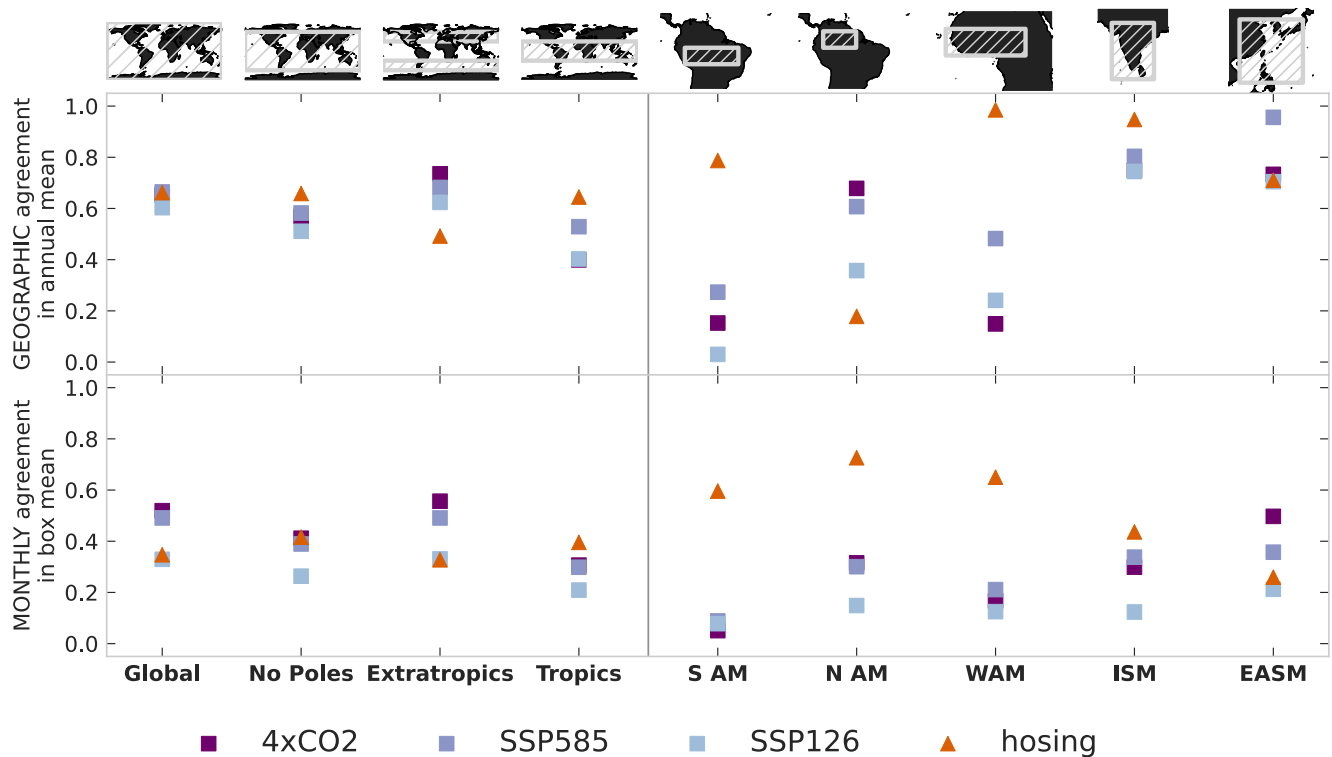
Figure 3. Model agreement in the North Atlantic Hosing Model Intercomparison Project experiments compared to the agreement in Climate Model Intercomparison Project warming experiments. (a) The fraction of gridcells in a given geographic region that agree on the sign of change in the annual mean rainfall. (b) The fraction of months in a year that agree on the sign of change in the mean monthly rainfall in the given box. The square markers show the agreement for the $4\times CO_2$ (purple), SSP585 (lilac), and SSP126 (light blue) experiments. The triangular orange marker shows the agreement of the hosing experiments. The regions of analysis are defined in Tables S1 and S2 in Supporting Information S1, and are shown as gray dashed boxes on the maps in the top row. A horizontal gray line separates the values for the global boxes from the regional monsoon boxes. The exact values are given in Tables S1 and S3 in Supporting Information S1.
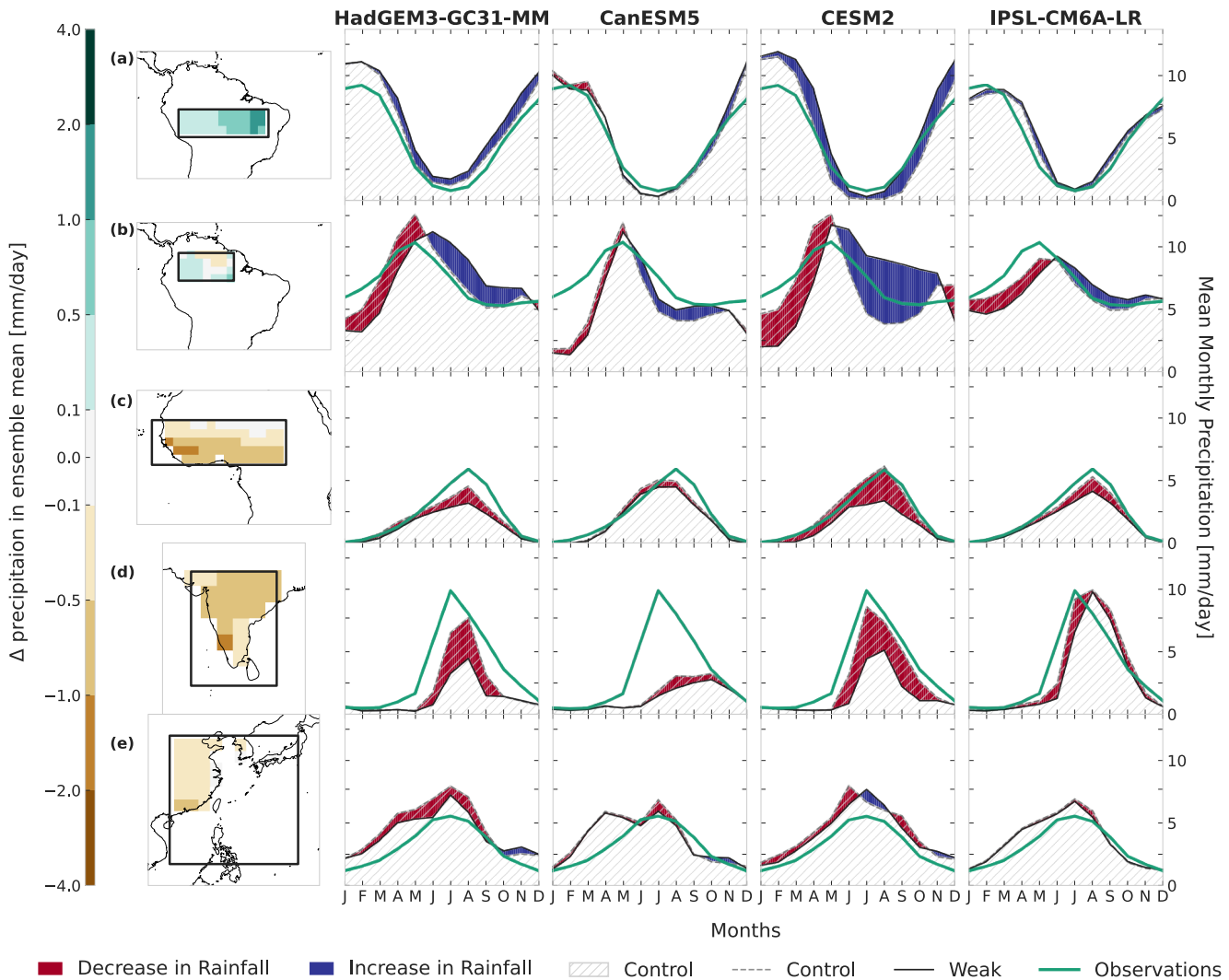
2.2. Changes in the Seasonal Cycle

Whilst the pattern of annual mean rainfall anomaly is informative for understanding the global effect of an AMOC collapse, the effect on the major tropical monsoon systems is by definition highly seasonally dependent. We investigate the seasonal change in rainfall in two ways. First, calculating the average seasonal cycle in the whole of a given monsoon region (Figure 5), and second, calculating the geographic pattern of change in dry and wet seasons in these regions (Figure 6). The seasonal cycle calculation is done in boxes that capture the most important part of the monsoon regions (see Table S2 for coordinates in Supporting Information S1). Because the SAM is spread across the equator, its northern and southern parts are affected differently by the collapse of the AMOC, and so we divide it at that line into two boxes. The detailed differences between the two regions are discussed later in this section, but it can already be seen from Figures 6a and 6c that the equator is indeed the dividing line in this region.

Because we analyze changes in the seasonal cycle from the piControl to the weak AMOC state, here we compare the seasonal cycle in the observations to that in the piControl run. This is not strictly an analysis of model bias, as the observations include anthropogenic forcings that are missing in the piControl runs. Rather, it is a statement on the starting point of the hosing experiments. All piControl model runs match the overall pattern of the observed seasonal rainfall, but there are considerable differences from observations in some cases (Figure 5). Their strengths depend on the region and model, with no model standing out as the closest one to the observations across regions. For example, the closest match between observations and control runs for the WAM and ISM is in CESM, but CanESM reproduces the southern Amazon rainfall better. CanESM, on the other hand, has the piControl run with the largest divergence from observations of any model in the northern Amazon and the ISM, with a difference of over 6 mm/day in the ISM wet season.

As discussed above, the sign of this monthly precipitation change is overall in agreement between models (Figure 3b and Figure S4b and Table S3 in Supporting Information S1). In general there is high agreement in the
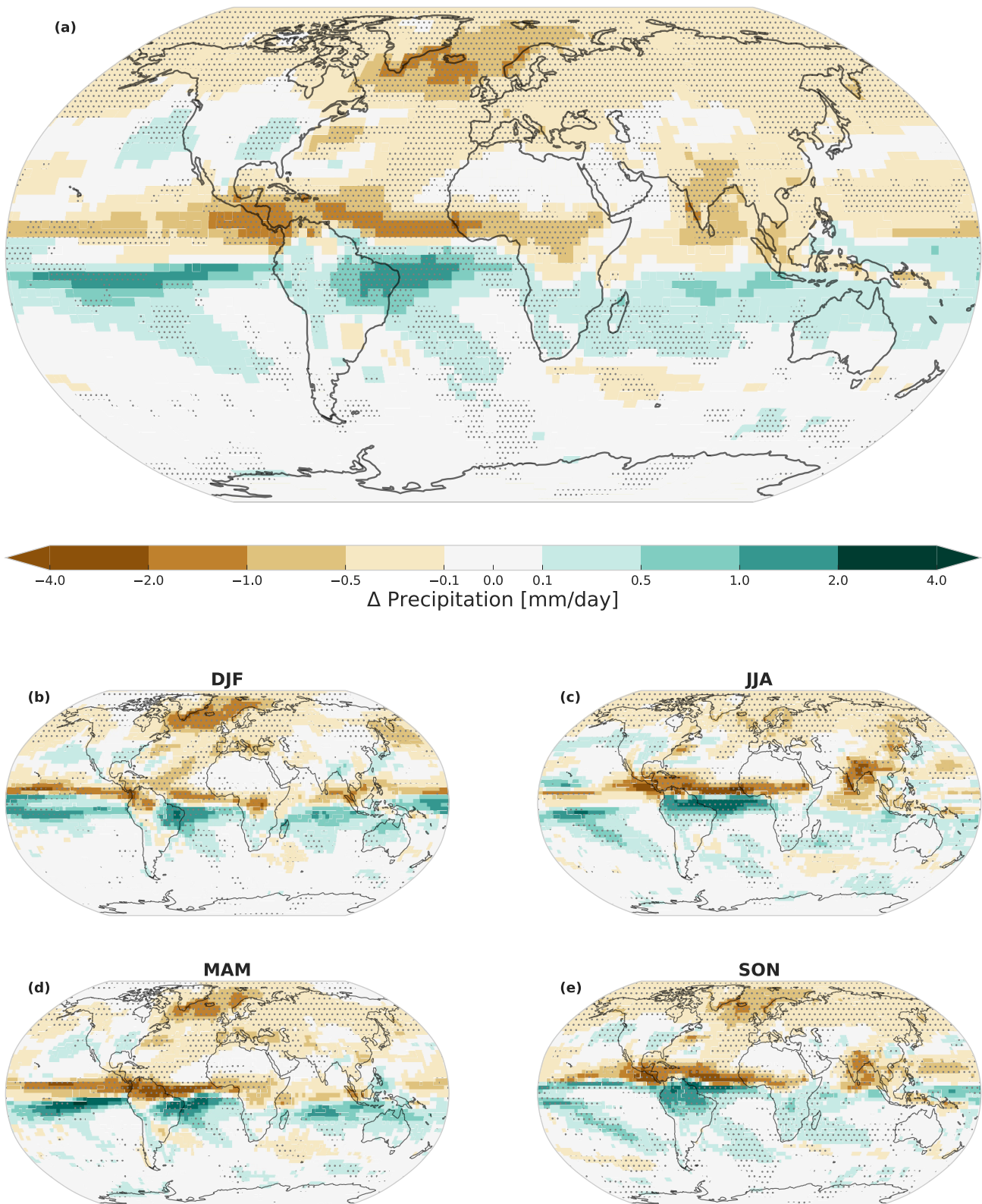
Figure 4. Average precipitation anomaly (weak Atlantic Meridional Overturning Circulation run minus piControl run) for the ensemble mean of the four models. Panel (a) shows the annual mean, whilst panels (b)–(e) show the season anomalies in DJF, JJA, MAM, and SON, respectively. We show MAM and SON in addition to the typical monsoon seasons to show how the monsoon in some regions can shift into these seasons. The stippling in each Figure indicates regions in which all four model anomalies agree in sign for that seasonal or annual mean.

Figure 5. Changes in the seasonal cycle due to an Atlantic Meridional Overturning Circulation (AMOC) collapse in two parts of the South American Monsoon (a, b), as well as in the West African Monsoon (c), Indian Summer Monsoon (d), and East Asian Summer Monsoon (e). The first column shows the ensemble mean average annual precipitation change in the given region (i.e., average over all four models). Taking this ensemble mean is justified by the high model agreement as identified in Figure 3. The remaining columns show the change in precipitation from the average seasonal cycle in the piControl (dot-dashed line) to the weak AMOC run (solid line) for the four different models. The area under the graph is shaded in red where the rainfall decreases and in blue where it increases in response to an AMOC collapse. The area common to both is marked by black hatches. The observed seasonal cycle in shown as the turquoise line. Coordinates for the monsoon boxes can be found in Table S2 in Supporting Information S1.

hosing experiments for the SAM and WAM and slightly less for the ISM and EASM, which is likely due to the former being directly impacted by the southward shift of the Atlantic ITCZ.

The pattern of seasonal cycle change present in these models is: (a) The southern Amazon gains a small amount of precipitation in all months, with the exception of CanESM showing a small precipitation decrease in the January-to-March part of the wet season (Figure 5a). The overall gains are in line with a southward shift of the Atlantic ITCZ, since this box extends from 5°S down to 15°S, that is, on the edge of the Atlantic ITCZ extent (Byrne et al., 2018) (Figure S5 in Supporting Information S1). A southward shift of the Atlantic ITCZ therefore brings more of the austral summer precipitation into this area; (b) The northern Amazon has a qualitative change in the seasonal cycle, with reduced rainfall in the piControl wet season and increased rainfall in the piControl dry season (Figure 5b). This is due to a combined shift in time of the wet season to later in the year and a reduction in the overall rainfall. It should be noted that this region also has a complex spatial pattern of changing rainfall in addition to the seasonal pattern (see Figures 2, 4, and 6); (c) The WAM has a clear pattern change (Figure 5c), showing decrease in rainfall during the wet season in all models. In CESM this is a 50% rainfall decrease, and in the other models closer to 5%–10%.
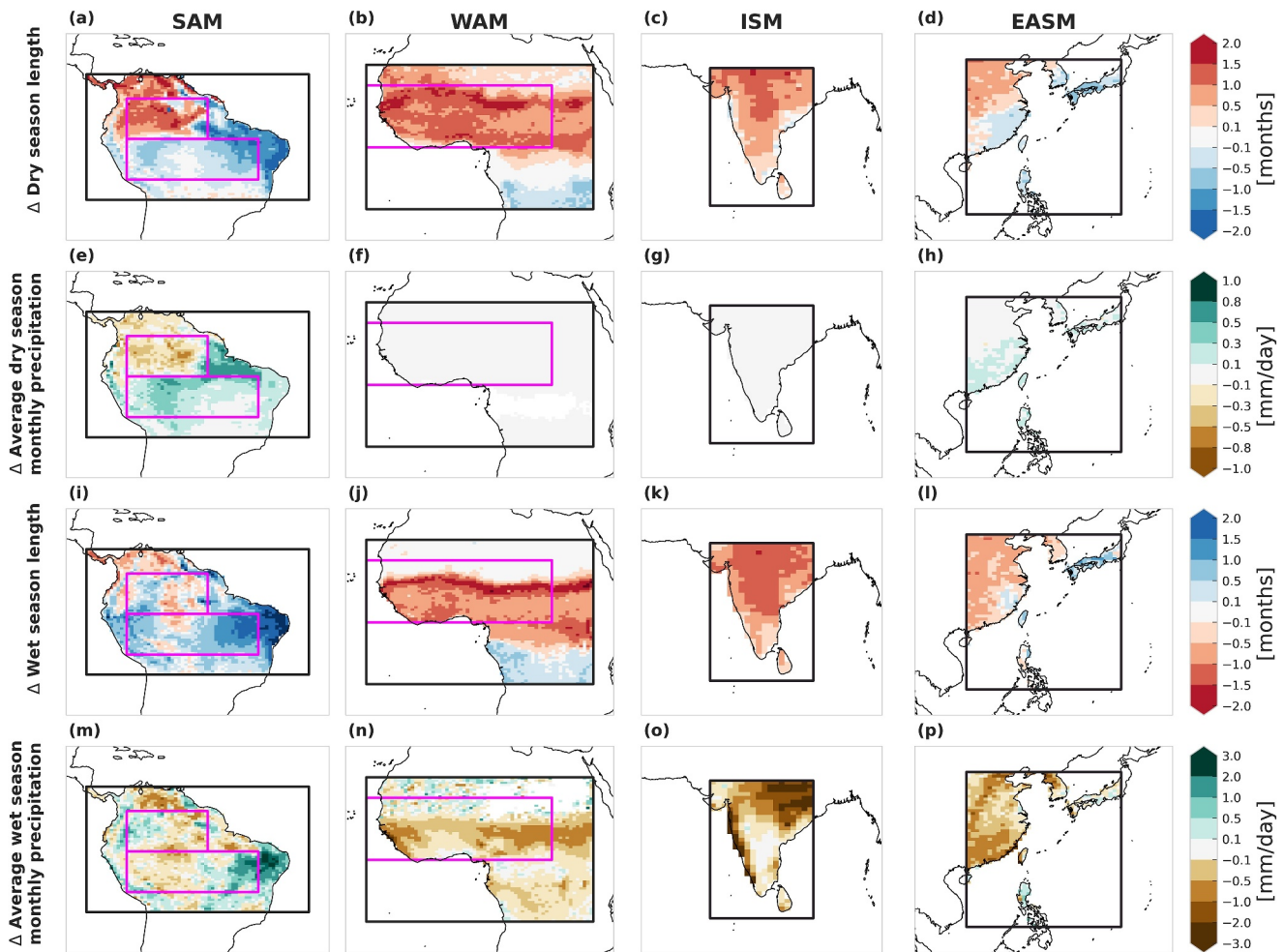
Figure 6. Changes in dry and wet season length and average monthly precipitation in HadGEM3-GC31-MM, defined as the weak Atlantic Meridional Overturning Circulation run value minus the piControl value. The four rows show the change in dry season length (a–d), average dry season monthly precipitation (e–h), wet season length (i–l) and average wet season monthly precipitation (m–p), respectively. Each column shows a different monsoon region, with the region used for defining the dry/wet season shown as a black box. See Section 4 for further details. The magenta boxes show the regions used in Figure 5 if they are different from the black boxes. Note the scales for the change in dry and wet season lengths are inverted to match red/blue to less/more rain respectively. Some areas within the monsoon regions are pure white if neither model run has a dry/wet season in that area, according to our definition (see Section 4). Coordinates of the boxes use to define the dry/wet season can be found in Table S4 in Supporting Information S1. Note that the dry season precipitation in the West African Monsoon and Indian Summer Monsoon is already close to zero, and thus the change is so small that all the results are between −0.1 and 0.1 in subplots (f) and (g).

Since the WAM is at the northern edge of the Atlantic ITCZ range (Figure S5 in Supporting Information S1), such a drying is to be expected from a southward shift of the ITCZ; (d) The ISM has a similar pattern change to the WAM, with a substantial loss of rainfall during the wet season (Figure 5d); and (e) The EASM shows a general drying which is relatively small in all models. All models also show a small increase in dry-season rainfall, but both these changes are too small to change the amplitude, timing, or structure of the overall seasonal cycle. CESM also shows a shift of the peak wet season rainfall from June to August (Figure 5e).

The magnitudes of all these changes in the different models are in line with the shift in the Atlantic ITCZ—the larger shift, the larger the precipitation change (see Figure S5 in Supporting Information S1 and Section 4 for details).

In the first column of Figure 5 and in Figure 2 it can be seen that while in general the sign of change is the same for the average as within the region, there is some spatial variation in the magnitude of the rainfall change. This spatial variation can be investigated through the change in the characteristics of the dry and wet seasons in the four regions. We define the dry (wet) season as the months with rainfall below (above) the 40th (60th) percentile of the whole region (see Section 4 for full details). Changes in dry- and wet-season rainfall and length caused by an

AMOC collapse are shown only for HadGEM for the sake of clarity, as it has the most realistic Atlantic ITCZ (see Figure S5 in Supporting Information S1) and highest spatial resolution (Figure 6). Note that the changes in precipitation in HadGEM are highly correlated with the changes in the other models in the monsoon regions (see Section 4 and Figures S7 and S8 in Supporting Information S1). The results agree with our previous findings: a general drying of the WAM, ISM and EASM through a longer dry season and a shorter wet season, and a more complex pattern for the SAM. In particular,

(i) the northern Amazon has a similar or longer dry season and a shorter wet season in most regions. The average dry season month also shows a reduction in precipitation. The wet season months are wetter in the western part, and drier in the eastern part, matching the pattern seen in the annual mean (Figure 2). However, HadGEM is the only model to show a reduction in rainfall over the eastern part of the northern Amazon (Figure S8 in Supporting Information S1);

(ii) the southern Amazon shows a shorter and wetter dry season, but has a mixed pattern for the wet season. The western part of the southern Amazon generally has a drier and shorter wet season. The overall increase in wet season rainfall is related to the longer and much wetter wet season of the eastern edge of the southern Amazon. All historical runs show a strong wet bias compared to observations in this southeastern Amazon region (Figure S1 in Supporting Information S1), so the change in rainfall might not be accurate;

(iii) in Africa, the WAM region is where the largest changes occur, with a longer dry season and a shorter wet season, especially at the southern edge of the Sahel. There is negligible change in the dry season monthly precipitation (which was already close to zero), but there is a reduction in the wet season precipitation. The only outlier is the Congo region, which benefits from a shorter dry season and a longer (but drier) wet season due to the southward shift of the Atlantic ITCZ;

(iv) for the ISM, the drying is more predominant in the wet season. While the dry season is longer by up to 1 month inland, the wet season is shorter by at least a month almost everywhere and has significantly drier months in the north-east;

(v) the EASM has a mixed change in the dry season: the northern part has a longer dry season with no change in precipitation, and the southern part has a shorter dry season with a small increase in the average precipitation. The overall drying is more drastic in the wet season, similarly to the ISM, with an overall shorter wet season and drier months.

We choose to show and discuss these two aspects of the seasonal cycle because we are interested in the tangible "on-the-ground" impacts of an AMOC collapse. Monsoon regions are often defined and investigated using wind speed and strength, but while those are important to the underlying physical mechanisms, for our purposes it is relevant to focus on the direct precipitation impacts. In addition, our focus on the seasonal cycle allows our results to be comparable with previous studies of the impact of an AMOC collapse on precipitation (Good et al., 2021; Parsons et al., 2014), and the discussion of dry/wet season length can be applicable to for example, studies on the Amazon forest (e.g., Carvalho et al., 2021). To allow comparison to the general monsoon literature we compute two classical and well-established monsoon indices: the Seasonal Normalized Seasonality (SNS) index and the Dynamic Normalized Seasonality (DNS) index (Li & Zeng, 2003). Roughly, the DNS is a way of comparing the angle between the given monthly wind vector and the climatological January wind vector (Li & Zeng, 2000). The SNS is similar, but compares the climatological July wind vector to the climatological January wind vector. A positive value of the indices corresponds to an angle larger than 90°, and regions with positive SNS values are used by Li and Zeng (2003) to define the extent of the global monsoon systems. These SNS-defined regions can be seen in Figure S9 in Supporting Information S1, and the seasonal variation of the DNS in Figure S10 in Supporting Information S1. Figure S9 in Supporting Information S1 shows why these indices are less useful for our purposes, as the core domain of the SAM is not included in the monsoon regions using this definition. In addition, in most models there is little change in the SNS-defined monsoon regions, even when the change in precipitation is large. The DNS is better at capturing the impacts, but as the reductions in its strength roughly correspond to decreased precipitation in the given month (compare Figure 5 and Figure S10 in Supporting Information S1), we choose to focus on Figure 5 and the direct precipitation impacts.

3. Discussion and Conclusions

The four monsoon systems investigated in this work are important parts of the global climate. More than half of the world's population is affected by monsoons (Moon & Ha, 2020; Wang et al., 2021), making them a high priority regarding possible impacts of anthropogenic global warming. This work is the first to compare the effect

of an AMOC collapse on monsoon systems in multiple CMIP6 model simulations with the same hosing conditions.

While the four models used in this study have different Atlantic ITCZ biases (Figure S5 in Supporting Information S1), their agreement on the pattern of the precipitation response to an AMOC collapse (Figure 3, Figures S4 and S7, and Tables S1 and S3 in Supporting Information S1) is a strong case for the robustness of that pattern (Figures 2 and 4).

The overall response structures are remarkably consistent across models, both geographically and seasonally (Figure S4 in Supporting Information S1). The WAM, ISM, and EASM show an overall drying with a shorter wet season and longer dry season in response to an AMOC collapse. The SAM shows a more spatially dependant pattern, with an overall annual increase in rainfall, a higher increase of annual precipitation and shorter dry season in the south and less pronounced change in the north. As our study uses model experiments in which there is no ongoing hosing and the AMOC is stable, these seasonal changes are unrelated to any seasonality in the hosing or the AMOC decline, and are only caused by the differences between the strong and weak AMOC states.

The year-long reduction in precipitation associated with WAM, ISM, and EASM would likely have severe ecological and socio-economic impacts. The effect of an AMOC collapse on the SAM and, hence, on the Amazon rainforest, is more uncertain. Parsons et al. (2014) showed that even with an overall decrease in yearly rainfall sums over the region, a shorter dry season can lead to increased productivity in the Amazon rainforest. However, the effect on the SAM dry season shown in this work is complex: in the northern Amazon, there is a shift of the seasonal cycle to later in the year in all models, and also an increase in dry season length. To understand the effect this would have on the rainforest requires additional modeling considering the vegetation response. On the other hand, the effect on the southern Amazon is different: more overall rainfall and a shortened and wetter dry season. This southern Amazon region is also the one shown to be losing resilience faster in the past decades (Boulton et al., 2022) and therefore may be more susceptible to changes in rainfall. This relative complexity in Amazon rainfall response may be the reason for the contrasting results of past models (Jackson et al., 2015; Stouffer et al., 2006) with regards to the effect of an AMOC collapse on the Amazon. The agreement of four different GCM experiments allows us to conclude that the overall effect of an AMOC collapse on the Amazon could counteract precipitation reductions projected for future global warming scenarios (see Arias et al., 2021).

Our work presents the effects of an AMOC collapse on monsoon precipitation, inferred from simulations of the NAHosMIP. Whilst the large-scale effects, such as a southward shift of the ITCZ, are well understood, there is still debate on the physical mechanisms that cause the precipitation changes in the individual monsoon regions (IPCC, 2022; Wassenburg et al., 2021). Since the SAM and WAM are directly adjacent to the Atlantic Ocean, the southward shift of the Atlantic ITCZ can explain most of the precipitation changes in these regions, as described above (see also Chang et al., 2008; Good et al., 2021). The situation for the ISM and EASM is more complex. Although some studies focus on localized effects such as the weakening of the local Hadley cell due to a weaker sea level pressure gradient (Sandeep et al., 2020; Sun et al., 2012), other studies investigate the pantropic teleconnections that link the changes in the Atlantic to Asian precipitation. Some of the suggested mechanisms include a southward shift of the sub-tropical jet (Marzin et al., 2013), a Matsuno-Gill-like response to Atlantic SST changes (Kucharski et al., 2009), or an atmospheric bridge connecting the Indian monsoon to north Atlantic SSTs through the upper troposphere (Kageyama et al., 2009). The weakening of the ISM and EASM has also been connected to a weakened walker circulation in the southern Pacific (Yu et al., 2009; Zhang & Delworth, 2005), although some studies show an opposite effect (Orihuela-Pinto et al., 2022). Testing these mechanisms in detail is beyond the scope of this study, but the NAHosMIP would provide a good base for further research of these debated mechanisms.

There is considerable uncertainty in the impact future global warming will have on monsoon rainfall (Arias et al., 2021; Moon & Ha, 2020; Wang et al., 2021). In this work we focus on the impacts of a potential AMOC collapse in pre-industrial climate, but it should be noted that in case of an AMOC collapse induced by global warming, the effects of a collapse on monsoon systems will combine with the effects of warmer temperatures. There are already some studies looking at this combined case (Bellomo et al., 2023; Chemison et al., 2022; W. Liu et al., 2020, 2017). In particular, Nian et al. (2023) investigated the effects an AMOC collapse would have on the stability of the Amazon rainforest at different levels of global mean temperature increase, and found that the collapse may delay or even prevent parts of the Amazon rainforest from dieback. In addition, we show that our models agree more for AMOC hosing experiments than they do for other CMIP6 warming experiments. Whilst

further work is needed on the combined effects of global warming and a collapse of the AMOC, our work will be helpful to constrain projections in at least part of this high-uncertainty region.

A key property of the impacts discussed in this work is that they persist for at least 100 years, and so are irreversible over a human lifetime. Whilst the direct impacts on monsoon rainfall from anthropogenic forcing could be reversed if the temperature is returned to pre-industrial levels, the collapse of the AMOC is permanent in the experiments considered in this study, something that was not certain in many previous hosing experiments (Jackson et al., 2015; Orihuela-Pinto et al., 2022; Stouffer et al., 2006). The impacts presented in this work could thus represent long-term changes that would persist even after a return to pre-industrial conditions.

Regardless of whether or not it is combined with increased temperatures, an AMOC collapse would result in a major rearranging of the global monsoon systems. This work shows that this rearrangement will have unfavorable effects on the WAM, ISM, and EASM and a more uncertain effect on the SAM and the Amazon rainforest.

4. Methods

4.1. Model Runs and Processing of the Outputs

We use the uniform hosing experiments from the North Atlantic Hosing Model Intercomparison study (NAHosMIP, Jackson et al., 2022). These experiments start from the respective pre-industrial control (piControl) runs of CMIP6 models, and apply a 0.3 Sv uniform hosing from 50°N to the Bering Strait. This hosing is applied for a given length of time and then stopped, after which the model continues to run. In the models we consider, the AMOC remains in the weak state after the hosing is turned off. For HadGEM, CanESM, and CESM, we use the u03-r50 experiments, in which the hosing has been halted after 50 years. For IPSL, we use the u03-r100 experiments, in which the hosing has been halted after 100 years.

For consistent comparison we use 80 years from each of the different model runs. As the AMOC takes a few years to settle into a stable state after the hosing is turned off, we take the last 80 years from HadGEM and CanESM, years 100–180 from CESM and years 60–140 from IPSL. For all models we use the first 80 years from the piControl.

For the comparison with the observational GPCP data set the model outputs are regridded to a regular 2.5° grid. For calculation of the ensemble mean the model outputs are regridded to the coarsest-resolution model grid, that of the CanESM5 model. When correlating the HadGEM3-GC31-MM output with the other three models, the HadGEM outputs are regridded to the respective model grid. All regridding is done using a first order conservative remapping.

4×CO$_2$ experiments are taken from the CMIP6 abrupt-4×CO$_2$ experiments, where an instantaneous quadrupling of the pre-industrial atmospheric CO$_2$ concentration is imposed and this concentration is kept constant. As the AMOC takes a few years to react to this we take years 60–140 from all models, using 80 years for consistent comparison with the NAHosMIP runs. We also use the full time period (1850–2014) of the CMIP6 historical runs, in which the anthropogenic forcings of 1850–2014 are applied to the climate, starting from some point in the piControl run. For the scenario-mip CMIP6 runs ssp585 and ssp126 we use years 2080–2100 for consistency across models. The ensemble members used from these various CMIP6 experiments are listed in Table S6 in Supporting Information S1.

4.2. Observational Data Sets

For comparison with model results and calculation of the ITCZ latitude (which requires precipitation data over land and sea), we use the GPCP Precipitation data provided by NOAA/OAR/ESRL PSL, Boulder, Colorado, USA (Adler et al., 2018) available for 1979–2020. For all other precipitation analyses we use the GPCC Full Data Monthly Product Version 2020 at 0.25° from 1921 to 2019 (the first 20 years are not used due to the paucity of measurements in the regions of interest) (U. Schneider et al., 2020).

For the observed AMOC strength (Figure S6 in Supporting Information S1) the RAPID AMOC monitoring project data is used (Frajka-Williams et al., 2021). For the wind strength used to calculate the SNS and DNS indices, we use the NCEP/NCAR Reanalysis Project data (Kalnay et al., 1996).

4.3. ITCZ Calculation

The ITCZ latitude is calculated following Good et al. (2021) to evaluate the model performance and the effect of an AMOC collapse.

The Atlantic ITCZ latitude is calculated in the area 35°W–15°W 15°S–15°N as a precipitation-weighted mean, as follows:

$$\phi_{itcz} = \sum_i \frac{P_{35-15°W,\phi_i} \cdot \phi_i}{P_{35-15°W,15°S-15°N}} \tag{1}$$

where $P_{35-15°W,\phi_i}$ is the zonally averaged precipitation at latitude ϕ_i, and $P_{35°W-15°W,\ 15°S-15°N}$ is the precipitation averaged over the whole region. Each latitude is thus weighted by the precipitation at that latitude.

The same procedure is repeated in the Indian and Pacific oceans for the following areas: 55°E–95°E, 15°S–15°N, and 120°E–95°W, 15°S–15°N, respectively.

4.4. The ITCZ and AMOC Strength in the Different Models

When compared to the observed seasonal cycle of the Atlantic ITCZ (hereafter simply ITCZ) the models can be divided into two groups (Figures S5a–S5d in Supporting Information S1): (a) The CanESM and IPSL piControl and historical runs have ITCZ latitudes going much further south (around 8°) in the December–March season (DJFM) than in observations. Their ITCZ varies more than 13° in latitude in a year, whilst the change in the average ITCZ seasonal cycle in the observations is 8.5°. It turns out that these two models only have a small (≤1°) latitudinal shift in the ITCZ between the control and weak AMOC; (b) HadGEM and CESM have a more realistic seasonal cycle of the ITCZ latitude, where the southward bias of the historical runs is about 1° for all months. Compared to the Atlantic Ocean, the biases in simulated ITCZ latitudes in the historical runs relative to the observations are smaller in the Indian and Pacific Oceans (see Figure S11 in Supporting Information S1).

On the other hand, those models which have a more realistic latitudinal shift are also those which have a stronger piControl and historical AMOC at 26.5N: In CanESM and IPSL the piControl and historical AMOC has a strength of 11.27 and 12.49 Sv respectively, and a post-hosing weak AMOC of 6.53 and 5.20 Sv (Figure S6 in Supporting Information S1). HadGEM and CESM, on the other hand, have a much stronger piControl and historical AMOC at 16.46 Sv and 17.39, respectively, and a post-hosing AMOC at 5.82 and 8.70 Sv. The RAPID array observational measurements of the AMOC strength at 26.5N have a mean of 16.9 ± 4.6 Sv in 2004–2020 (Frajka-Williams et al., 2021), closer to HadGEM and CESM than to the other two models. Note, however, that these are historical observations and thus include the effect of anthropogenic forcings, and cannot be directly compared with the piControl simulations.

However, although the collapsed AMOC has a similar strength in all four models, there are still major differences between the post-collapsed ITCZ cycles of the two groups of models. It is more likely that other properties of the IPSL and CanESM models cause both an extended ITCZ excursion to the south and a weaker piControl and historical AMOC. In the CMIP6 Atmospheric Model Intercomparison Project (AMIP) experiments CanESM and IPSL have a seasonal ITCZ cycle much closer to the observations, without the southward excursion (Figure S12 in Supporting Information S1). As the AMIP models are forced with historical observed SSTs, the differences from observations in the historical and piControl runs of CanESM and IPSL are likely due to either biases in the modeled SST fields or in the SST-precipitation interactions in these models. Thus, for a reliable estimate of the magnitude (and not only the sign) of the precipitation change due to an AMOC collapse, further work should focus on the differences in the AMOC and SST biases of the different models.

4.5. Defining Dry and Wet Seasons

The dry and wet seasons are defined using a non-parametric approach for consistency across monsoon regions. First, percentile boundaries are calculated for each region using all gridpoints and years. The dry or wet season months in a given year and gridpoint are then all the months that have less or more rain than the chosen percentile boundary of the region. The 40th and 60th percentile are chosen for the dry and wet season, respectively. The dry season percentile is chosen such that for the SAM the dry season monthly rainfall limit is about 100 mm, which is

the mean monthly evapotranspiration value of tropical forests (below this value evapotranspiration exceeds rainfall, see Carvalho et al. (2021)).

The averaged dry (wet) season length is then the mean of dry (wet) season length over all years. The total dry (wet) season precipitation is, accordingly, the sum of rainfall in all months of the season, which is again averaged over all years to give the average total dry (wet) season precipitation. However, when comparing seasonal rainfall across runs with different season lengths, the total precipitation will be biased by the difference in season length. An average dry (wet) season monthly precipitation value is therefore defined by dividing the total dry (wet) season rainfall in a year by the length of the dry (wet) season in that year, and the average is calculated as

$$p_{i,\mathrm{dry,avg}} = \frac{1}{T}\sum_{t=1}^{T}\frac{p_{i,t,\mathrm{dry}}}{x_{i,t,\mathrm{dry}}}, \tag{2}$$

where $p_{i,t,\mathrm{dry}}$ and $x_{i,t,\mathrm{dry}}$ are respectively the total dry season precipitation and dry season length in grid-point i in year t, and the sum is over all years T.

When comparing these values between the piControl and weak AMOC model runs, there are two ways to define the dry (wet) season for the weak AMOC run. The first is to use the regions' percentile boundary values calculated for the piControl run, and apply them as the limit defining the weak AMOC seasons. The second is to independently calculate new percentiles for the weak AMOC precipitation and use those as the defining limits. The first option reflects the experience of an abrupt change in the AMOC, as it shows how the "known" seasons would change after a collapse. The second is more applicable to an analysis of a long-term state, as it shows what the dry (wet) season would look like in a world with a weak AMOC. As we are interested in the effect of an abrupt collapse on ecosystems and societies which are in general adapted to a given pattern and strength of seasonal rainfall, the value of interest will be the first one, which reflects how the known seasons would change.

4.6. The SNS and DNS Indices

We calculate the SNS and DNS indices following Li and Zeng (2003), and in particular Equation 2 from that paper for the monthly climatology DNS and Equation 3 from that paper for the SNS. All our calculations are for the 850 hPa level of the wind fields. The SNS-defined monsoon regions are the same as in Li and Zeng (2003): regions in which the SNS is larger than 0.

4.7. Model Bias

Figure S1 in Supporting Information S1 shows the difference between the CMIP6 historical run for the four models and the global GPCP observations. The pattern in the yearly averaged precipitation bias is as follows: (a) For the SAM all models except HadGEM show an ∼2 mm/day dry bias, whilst HadGEM shows a weak wet bias in the southern Amazon and a weak dry bias in the northern Amazon; (b) For the WAM there is a small dry bias in all four models; (c) For the ISM HadGEM and CanESM have a dry bias everywhere, whilst CESM and IPSL have a dry bias in the north and a wet bias in the south; (d) For the EASM all models except IPSL have a wet bias, whilst IPSL has a small dry bias. Note that, to discuss biases, we compare the observations with the historical runs. This is different from the comparisons for the post-hosing, collapsed AMOC state, which we compare with the piControl runs. In the latter case there are no anthropogenic forcings present.

4.8. Agreement Between HadGEM3-GC31-MM and Other Models

In Figure 6 the changes in dry and wet seasons are shown only for HadGEM. This model was chosen due to its realistic Atlantic ITCZ and its higher spatial resolution. To justify the use of HadGEM as representative of all models, Figure S8 in Supporting Information S1 shows the regions in which all three other models or two of the other three models show the same sign of precipitation anomaly as HadGEM, and Table S5 in Supporting Information S1 shows the correlation of the other models with HadGEM. These figures show the remarkable agreement between the models. The only region in the monsoon areas of interest where HadGEM does not agree with the other models is in the northeastern Amazon, where HadGEM shows a slight overall drying. However, it can be seen that the detailed seasonal response of precipitation in that region is the same in all four models (Figure 5). The annual mean in this region is the combined effect of a drying in January to June and increased

rainfall in the rest of the year. HadGEM also has drying in January to June and an increase in rainfall during the rest of the year, but these two effects do not balance each other the same way as in the other models, so that the annual mean ends up behaving differently.

Data Availability Statement

The AMOC data from the NAHosMIP is available at Jackson et al. (2023), and any other NAHosMIP data is available upon reques All the CMIP6 experimental data is available via the Earth System Grid Federation (ESGF) servers at https://aims2.llnl.gov/search/?project=CMIP6 (Eyring et al., 2016). The GPCP and GPCC precipitation datasets are available at Adler et al. (2016) and U. Schneider et al. (2020), respectively. The RAPID observational data is available at Frajka-Williams et al. (2021). The wind data from NCEP-NCAR Reanalysis 1 data is provided by the NOAA PSL, Boulder, Colorado, USA, from their website at https://psl.noaa.gov/data/gridded/data.ncep.reanalysis.html (Kalnay et al., 1996). Code for this manuscript is available at https://doi.org/10.5281/zenodo.13327366 (github link: github.com/mayaby/NAHosMIP_monsoons).

References

Adler, R., Sapiano, M. R. P., Huffman, G. J., Wang, J.-J., Gu, G., Bolvin, D., et al. (2018). The global precipitation climatology project (GPCP) monthly analysis (new version 2.3) and a review of 2017 global precipitation. *Atmosphere*, *9*(4), 138. https://doi.org/10.3390/atmos9040138

Adler, R., Wang, J.-J., Sapiano, M., Huffman, G., Chiu, L., Xie, P. P., et al. (2016). Global precipitation climatology project (GPCP) climate data record (CDR) [Dataset]. *National Centers for Environmental Information*. https://doi.org/10.7289/V56971M6

Arias, P. A., Bellouin, N., Coppola, E., Jones, R. G., Krinner, G., Marotzke, J., et al. (2021). Technical summary. In V. Masson-Delmotte, P. Zhai, A. Pirani, S. L. Connors, C. Péan, S. Berger, et al. (Eds.), *Climate change 2021: The physical science basis. Contribution of working group I to the sixth assessment report of the intergovernmental panel on climate change (chapter 1)*. Retrieved from https://www.ipcc.ch/report/ar6/wg1/downloads/report/IPCC_AR6_WGI_TS.pdf

Bellomo, K., Mehling, O., Torino, P., Bellomo, K., & Mehling, O. (2023). Impacts and state-dependence of AMOC weakening in a warming climate Impacts and state-dependence of AMOC weakening in a warming climate from climate model simulations. *Geophysical Research Letters*, *51*, e2023GL107624. https://doi.org/10.1029/2023GL107624

Ben-Yami, M., Skiba, V., Bathiany, S., & Boers, N. (2023). Uncertainties in critical slowing down indicators of observation-based fingerprints of the Atlantic Overturning Circulation. *Nature Communications*, *14*, 1–11. https://doi.org/10.1038/s41467-023-44046-9

Boers, N. (2021). Observation-based early-warning signals for a collapse of the atlantic meridional overturning circulation. *Nature Climate Change*, *11*(8), 680–688. https://doi.org/10.1038/s41558-021-01097-4

Boulton, C. A., Lenton, T. M., & Boers, N. (2022). Pronounced loss of Amazon rainforest resilience since the early 2000s. *Nature Climate Change*, *12*(March), 271–278. https://doi.org/10.1038/s41558-022-01287-8

Bryden, H. L., Longworth, H. R., & Cunningham, S. A. (2005). Slowing of the Atlantic meridional overturning circulation at 25°N. *Nature*, *438*(7068), 655–657. https://doi.org/10.1038/nature04385

Byrne, M. P., Pendergrass, A. G., Rapp, A. D., & Wodzicki, K. R. (2018). Response of the intertropical convergence zone to climate change: Location, width, and strength. *Current Climate Change Reports*, *4*(4), 355–370. https://doi.org/10.1007/s40641-018-0110-5

Caesar, L., McCarthy, G. D., Thornalley, D. J., Cahill, N., & Rahmstorf, S. (2021). Current atlantic meridional overturning circulation weakest in last millennium. *Nature Geoscience*, *14*(3), 118–120. https://doi.org/10.1038/s41561-021-00699-z

Caesar, L., Rahmstorf, S., Robinson, A., Feulner, G., & Saba, V. (2018). Observed fingerprint of a weakening Atlantic Ocean overturning circulation. *Nature*, *556*(7700), 191–196. https://doi.org/10.1038/s41586-018-0006-5

Carvalho, N. S., Anderson, L. O., Nunes, C. A., Pessôa, A. C., Silva Junior, C. H., Reis, J. B., et al. (2021). Spatio-Temporal variation in dry season determines the Amazonian fire calendar. *Environmental Research Letters*, *16*(12), 125009. https://doi.org/10.1088/1748-9326/ac3aa3

Chang, P., Zhang, R., Hazeleger, W., Wen, C., Wan, X., Ji, L., et al. (2008). Oceanic link between abrupt changes in the north Atlantic Ocean and the African monsoon. *Nature Geoscience*, *1*(7), 444–448. https://doi.org/10.1038/ngeo218

Chemison, A., Defrance, D., Ramstein, G., & Caminade, C. (2022). Impact of an acceleration of ice sheet melting on monsoon systems. *Earth System Dynamics*, *13*(3), 1259–1287. https://doi.org/10.5194/esd-13-1259-2022

Defrance, D., Ramstein, G., Charbit, S., Vrac, M., Famien, A. M., Sultan, B., et al. (2017). Consequences of rapid ice sheet melting on the Sahelian population vulnerability. *Proceedings of the National Academy of Sciences of the United States of America*, *114*(25), 6533–6538. https://doi.org/10.1073/pnas.1619358114

Donohoe, A., Marshall, J., Ferreira, D., & Mcgee, D. (2013). The relationship between ITCZ location and cross-equatorial atmospheric heat transport: From the seasonal cycle to the last glacial maximum. *Journal of Climate*, *26*(11), 3597–3618. https://doi.org/10.1175/JCLI-D-12-00467.1

Drijfhout, S. S., Weber, S. L., & van der Swaluw, E. (2011). The stability of the MOC as diagnosed from model projections for pre-industrial, present and future climates. *Climate Dynamics*, *37*(7–8), 1575–1586. https://doi.org/10.1007/s00382-010-0930-z

Eyring, V., Bony, S., Meehl, G. A., Senior, C. A., Stevens, B., Stouffer, R. J., & Taylor, K. E. (2016). Overview of the coupled model intercomparison project phase 6 (CMIP6) experimental design and organization. *Geoscientific Model Development*, *9*(5), 1937–1958. https://doi.org/10.5194/gmd-9-1937-2016

Fiedler, S., Crueger, T., D'Agostino, R., Peters, K., Becker, T., Leutwyler, D., et al. (2020). Simulated tropical precipitation assessed across three major phases of the coupled model intercomparison project (CMIP). *Monthly Weather Review*, *148*(9), 3653–3680. https://doi.org/10.1175/MWR-D-19-0404.1

Frajka-Williams, E., Moat, B., Smeed, D., Rayner, D., Johns, W., Baringer, M., et al. (2021). Atlantic meridional overturning circulation observed by the rapid-mocha-wbts (rapid-meridional overturning circulation and heatflux array-western boundary time series) array at 26n from 2004 to 2020 (v2020.1) [Dataset]. *British Oceanographic Data Centre-Natural Environment Research Council*. https://doi.org/10.5285/cc1e34b3-3385-662b-e053-6c86abc03444

Frierson, D. M., Hwang, Y. T., Fučkar, N. S., Seager, R., Kang, S. M., Donohoe, A., et al. (2013). Contribution of ocean overturning circulation to tropical rainfall peak in the Northern Hemisphere. *Nature Geoscience*, *6*(11), 940–944. https://doi.org/10.1038/ngeo1987

Good, P., Boers, N., Boulton, C. A., Lowe, J. A., & Richter, I. (2021). How might a collapse in the atlantic meridional overturning circulation affect rainfall over tropical South America? In *Climate resilience and sustainability (November)* (pp. 1–13). https://doi.org/10.1002/cli2.26

Guiling, W., Kazi, F., Liangzhi, Y., Miao, Y., Jeremy, P., & Zhenming, J. (2017). Projecting regional climate and cropland changes using a linked biogeophysical-socioeconomic modelin. *Journal of Advances in Modeling Earth Systems*, *8*, 1180–1209. https://doi.org/10.1002/2016MS000903

Häggi, C., Chiessi, C. M., Merkel, U., Mulitza, S., Prange, M., Schulz, M., & Schefuß, E. (2017). Response of the Amazon rainforest to late Pleistocene climate variability. *Earth and Planetary Science Letters*, *479*, 50–59. https://doi.org/10.1016/j.epsl.2017.09.013

Henry, L. G., McManus, J. F., Curry, W. B., Roberts, N. L., Piotrowski, A. M., & Keigwin, L. D. (2016). North Atlantic Ocean circulation and abrupt climate change during the last glaciation. *Science*, *353*(6298), 470–474. https://doi.org/10.1126/science.aaf5529

IPCC. (2022). Extremes, abrupt changes and managing risks. In *The ocean and cryosphere in a changing climate: Special report of the intergovernmental panel on climate change* (pp. 589–656). Cambridge University Press.

Jackson, L. C., Alastue de Asenjo, E., Bellomo, K., Danabasoglu, G., Hu, A., Jungclaus, J., et al. (2023). Nahosmip data [Dataset]. *Zenodo*. https://doi.org/10.5281/zenodo.7643437

Jackson, L. C., Asenjo, E. A. D., Bellomo, K., Danabasoglu, G., Haak, H., Hu, A., et al. (2022). Understanding AMOC stability: The North Atlantic hosing model intercomparison project. In *Geoscientific model development discussions (November)* (pp. 1–32). https://doi.org/10.5194/gmd-2022-277

Jackson, L. C., Kahana, R., Graham, T., Ringer, M. A., Woollings, T., Mecking, J. V., & Wood, R. A. (2015). Global and European climate impacts of a slowdown of the AMOC in a high resolution GCM. *Climate Dynamics*, *45*(11–12), 3299–3316. https://doi.org/10.1007/s00382-015-2540-2

Jackson, L. C., Roberts, M. J., Hewitt, H. T., Iovino, D., Koenigk, T., Meccia, V. L., et al. (2020). Impact of ocean resolution and mean state on the rate of AMOC weakening. *Climate Dynamics*, *55*(7–8), 1711–1732. https://doi.org/10.1007/s00382-020-05345-9

Jackson, L. C., & Wood, R. A. (2018). Hysteresis and resilience of the AMOC in an eddy-permitting GCM. *Geophysical Research Letters*, *45*(16), 8547–8556. https://doi.org/10.1029/2018GL078104

Kageyama, M., Mignot, J., Swingedouw, D., Marzin, C., Alkama, R., & Marti, O. (2009). Glacial climate sensitivity to different states of the Atlantic meridional overturning circulation: Results from the IPSL model. *Climate of the Past*, *5*(3), 551–570. https://doi.org/10.5194/cp-5-551-2009

Kalnay, E., Collins, W., Deaven, D., Gandin, L., Iredell, M., Jenne, R., & Joseph, D. (1996). The NCEP NCAR 40-year reanalysis project. 1996. pdf. *Bulletin of the American Meteorological Society*, *77*(3), 437–472. https://doi.org/10.1175/1520-0477(1996)077%3C0437%3ATNYRP%3E2.0.CO%3B2

Kilbourne, K. H., Wanamaker, A. D., Moffa-Sanchez, P., Reynolds, D. J., Amrhein, D. E., Butler, P. G., et al. (2022). Atlantic circulation change still uncertain. *Nature Geoscience*, *15*(3), 13–16. https://doi.org/10.1038/s41561-022-00896-4

Kucharski, F., Bracco, A., Yoo, J. H., Tompkins, A. M., Feudale, L., Ruti, P., & Dell'Aquila, A. (2009). A Gill-Matsuno-type mechanism explains the tropical Atlantic influence on African and Indian monsoon rainfall. *Quarterly Journal of the Royal Meteorological Society*, *135*(640), 569–579. https://doi.org/10.1002/qj.406

Latif, M., Sun, J., Visbeck, M., & Hadi Bordbar, M. (2022). Natural variability has dominated atlantic meridional overturning circulation since 1900. *Nature Climate Change*, *12*(5), 455–460. https://doi.org/10.1038/s41558-022-01342-4

Lee, J. Y., Marotzke, J., Bala, G., Cao, L., Corti, S., Dunne, J. P., et al. (2021). Future global climate: Scenario-based projections and near-term information. In V. Masson-Delmotte, P. Zhai, A. Pirani, S. L. Connors, C. Péan, S. Berger, et al. (Eds.), *Climate change 2021: The physical science basis. Contribution of working group I to the sixth assessment report of the intergovernmental panel on climate change (chap. 4)*. Retrieved from https://www.ipcc.ch/report/ar6/wg1/downloads/report/IPCC_AR6_WGI_Chapter_04.pdf

Li, J., & Zeng, Q. (2000). Significance of the normalized seasonality of wind field and its rationality for characterizing the monsoon. *Science in China Series D: Earth Sciences*, *43*(6), 651–653. https://doi.org/10.1007/bf02879509

Li, J., & Zeng, Q. (2003). A new monsoon index and the geographical monsoons distribution of the global monsoons. *Advances in Atmospheric Sciences*, *20*(2), 299–302. https://doi.org/10.1007/s00376-003-0016-5

Liu, W., Fedorov, A. V., Xie, S. P., & Hu, S. (2020). Climate impacts of a weakened Atlantic meridional overturning circulation in a warming climate. *Science Advances*, *6*(26), 2–10. https://doi.org/10.1126/sciadv.aaz4876

Liu, W., Xie, S. P., Liu, Z., & Zhu, J. (2017). Overlooked possibility of a collapsed Atlantic meridional overturning circulation in warming climate. *Science Advances*, *3*(1), 1–8. https://doi.org/10.1126/sciadv.1601666

Liu, Y., Chiang, J. C., Chou, C., & Patricola, C. M. (2014). Atmospheric teleconnection mechanisms of extratropical North Atlantic SST influence on Sahel rainfall. *Climate Dynamics*, *43*(9–10), 2797–2811. https://doi.org/10.1007/s00382-014-2094-8

Marzin, C., Kallel, N., Kageyama, M., Duplessy, J. C., & Braconnot, P. (2013). Glacial fluctuations of the Indian monsoon and their relationship with North Atlantic climate: New data and modelling experiments. *Climate of the Past*, *9*(5), 2135–2151. https://doi.org/10.5194/cp-9-2135-2013

Moon, S., & Ha, K. J. (2020). Future changes in monsoon duration and precipitation using CMIP6. *npj Climate and Atmospheric Science*, *3*(1), 1–7. https://doi.org/10.1038/s41612-020-00151-w

Mosblech, N. A., Bush, M. B., Gosling, W. D., Hodell, D., Thomas, L., Van Calsteren, P., et al. (2012). North Atlantic forcing of Amazonian precipitation during the last ice age. *Nature Geoscience*, *5*(11), 817–820. https://doi.org/10.1038/ngeo1588

Nian, D., Bathiany, S., Ben-Yami, M., Blaschke, L. L., Hirota, M., Rodrigues, R. R., & Boers, N. (2023). A potential collapse of the Atlantic Meridional Overturning Circulation may stabilise eastern Amazonian rainforests. *Communications Earth and Environment*, *4*(1), 1–11. https://doi.org/10.1038/s43247-023-01123-7

Orihuela-Pinto, B., England, M. H., & Taschetto, A. S. (2022). Interbasin and interhemispheric impacts of a collapsed atlantic overturning circulation. *Nature Climate Change*, *12*(6), 558–565. https://doi.org/10.1038/s41558-022-01380-y

Parsons, L. A., Yin, J., Overpeck, J. T., Stouffer, R. J., & Malyshev, S. (2014). Influence of the Atlantic meridional overturning circulation on the monsoon rainfall and carbon balance of the American tropics. *Geophysical Research Letters*, *41*(1), 146–151. https://doi.org/10.1002/2013GL058454

Rahmstorf, S. (2002). NAT(419,207)-circulation. *Nature*, *419*(September), 207–214. https://doi.org/10.1038/nature01090

Rahmstrof, S., Crucifix, M., Ganopolski, A., Goosse, H., Kamenkovich, I., Knutti, R., et al. (2005). Thermohaline circulation hysteresis: A model intercomparison. *Geophysical Research Letters*, *32*(23), 1–5. https://doi.org/10.1029/2005GL023655

Romanou, A., Rind, D., Jonas, J., Miller, R., Kelley, M., Russell, G., et al. (2023). Stochastic bifurcation of the North Atlantic circulation under A mid-range future climate scenario with the NASA-GISS ModelE. *Journal of Climate*, *36*(18), 1–49. https://doi.org/10.1175/JCLI-D-22-0536

Sandeep, N., Swapna, P., Krishnan, R., Farneti, R., Prajeesh, A. G., Ayantika, D. C., & Manmeet, S. (2020). South Asian monsoon response to weakening of Atlantic meridional overturning circulation in a warming climate. *Climate Dynamics*, *54*(7–8), 3507–3524. https://doi.org/10.1007/s00382-020-05180-y

Schneider, T., Bischoff, T., & Haug, G. H. (2014). Migrations and dynamics of the intertropical convergence zone. *Nature*, *513*(7516), 45–53. https://doi.org/10.1038/nature13636

Schneider, U., Becker, A., Finger, P., Rustemeier, E., & Ziese, M. (2020). Gpcc full data monthly product version 2020 at 0.25°: Monthly land-surface precipitation from rain-gauges built on gts-based and historical data [Dataset]. *Physical Sciences Laboratory*. https://doi.org/10.5676/DWD_GPCC/FD_M_V2020_025

Stommel, H. (1961). Thermohaline convection with two stable regimes of flow. *Tellus*, *13*(2), 224–230. https://doi.org/10.3402/tellusa.v13i2.9491

Stouffer, R. J., Yin, J., Gregory, J. M., Dixon, K. W., Spelman, M. J., Hurlin, W., et al. (2006). Investigating the causes of the response of the thermohaline circulation to past and future climate changes. *Journal of Climate*, *19*(8), 1365–1387. https://doi.org/10.1175/JCLI3689.1

Strandberg, G., & Lind, P. (2021). The importance of horizontal model resolution on simulated precipitation in Europe—From global to regional models. *Weather and Climate Dynamics*, *2*(1), 181–204. https://doi.org/10.5194/wcd-2-181-2021

Sun, Y., Clemens, S. C., Morrill, C., Lin, X., Wang, X., & An, Z. (2012). Influence of Atlantic meridional overturning circulation on the East Asian winter monsoon. *Nature Geoscience*, *5*(1), 46–49. https://doi.org/10.1038/ngeo1326

Wang, B., Biasutti, M., Byrne, M. P., Castro, C., Chang, C. P., Cook, K., et al. (2021). Monsoons climate change assessment. *Bulletin of the American Meteorological Society*, *102*(1), E1–E19. https://doi.org/10.1175/BAMS-D-19-0335.1

Wassenburg, J. A., Vonhof, H. B., Cheng, H., Martínez-García, A., Ebner, P. R., Li, X., et al. (2021). Penultimate deglaciation Asian monsoon response to North Atlantic circulation collapse. *Nature Geoscience*, *14*(12), 937–941. https://doi.org/10.1038/s41561-021-00851-9

Weijer, W., Cheng, W., Drijfhout, S. S., Fedorov, A. V., Hu, A., Jackson, L. C., et al. (2019). Stability of the Atlantic meridional overturning circulation: A review and synthesis. *Journal of Geophysical Research: Oceans*, *124*(8), 5336–5375. https://doi.org/10.1029/2019JC015083

WRCP, W. C. R. P. (2023). The global monsoon systems. Retrieved from https://www.wcrp-climate.org/documents/monsoon_factsheet.pdf

Yu, L., Gao, Y. Q., Wang, H. J., Guo, D., & Li, S. L. (2009). The responses of east Asian summer monsoon to the North Atlantic meridional overturning circulation in an enhanced freshwater input simulation. *Chinese Science Bulletin*, *54*(24), 4724–4732. https://doi.org/10.1007/s11434-009-0720-3

Zhang, R., & Delworth, T. L. (2005). Simulated tropical response to a substantial weakening of the Atlantic (2002) (pp. 1853–1860).

Zhu, C., Liu, Z., Zhang, S., & Wu, L. (2023). Likely accelerated weakening of Atlantic overturning circulation emerges in optimal salinity fingerprint. *Nature Communications*, *14*(1), 1–9. https://doi.org/10.1038/s41467-023-36288-4